
EMPLOYING VECTOR FIELD TECHNIQUES ON THE ANALYSIS OF MEMRISTOR CELLULAR NONLINEAR NETWORKS CELL DYNAMICS

PRESENTED CONFERENCE PAPER

Chandan Singh

Faculty of Electrical and Computer Engineering
Technische Universität Dresden
Dresden, Germany
chandan_omprakash.singh@mailbox.tu-dresden.de

Vasileios Ntinias*

Faculty of Electrical and Computer Engineering
Technische Universität Dresden
Dresden, Germany
vasileios.ntinas@tu-dresden.de

Dimitrios Prousalis

Faculty of Electrical and Computer Engineering
Technische Universität Dresden
Dresden, Germany
dimitrios.prousalis@tu-dresden.de

Yongmin Wang

Peter Grünberg Institut (PGI-10)
Forschungszentrum Jülich GmbH
Jülich, Germany
yon.wang@fz-juelich.de

Ahmet Samil Demirkol

Faculty of Electrical and Computer Engineering
Technische Universität Dresden
Dresden, Germany
ahmet_samil.demirkol@tu-dresden.de

Ioannis Messaris

Faculty of Electrical and Computer Engineering
Technische Universität Dresden
Dresden, Germany
ioannis.messariss@tu-dresden.de

Vikas Rana

Peter Grünberg Institut (PGI-10)
Forschungszentrum Jülich GmbH
Jülich, Germany
v.rana@fz-juelich.de

Stephan Menzel

Peter Grünberg Institut (PGI-7)
Forschungszentrum Jülich GmbH
Jülich, Germany
st.menzel@fz-juelich.de

Alon Ascoli

Faculty of Electrical and Computer Engineering
Technische Universität Dresden
Dresden, Germany
alon.ascoli@tu-dresden.de

Ronald Tetzlaff

Faculty of Electrical and Computer Engineering
Technische Universität Dresden
Dresden, Germany
ronald.tetzlaff@tu-dresden.de

September 30, 2023

ABSTRACT

This paper introduces an innovative graphical analysis tool for investigating the dynamics of Memristor Cellular Nonlinear Networks (M-CNNs) featuring 2nd-order processing elements, known as M-CNN cells. In the era of specialized hardware catering to the demands of intelligent autonomous systems, the integration of memristors within Cellular Nonlinear Networks (CNNs) has emerged as a promising paradigm due to their exceptional characteristics. However, the standard Dynamic Route Map (DRM) analysis, applicable to 1st-order systems, fails to address the intricacies of 2nd-order

*Presented at the 18th IEEE International Workshop on Cellular Nanoscale Networks and their Applications (CNNA'23) and the 8th Memristor and Memristive Symposium.

M-CNN cell dynamics, as well the 2nd-order DRM (DRM2) exhibits limitations on the graphical illustration of local dynamical properties of the M-CNN cells, e.g. state derivative's magnitude. To address this limitation, we propose a novel integration of M-CNN cell vector field into the cell's phase portrait, enhancing the analysis efficacy and enabling efficient M-CNN cell design. A comprehensive exploration of M-CNN cell dynamics is presented, showcasing the utility of the proposed graphical tool for various scenarios, including bistable and monostable behavior, and demonstrating its superior ability to reveal subtle variations in cell behavior. Through this work, we offer a refined perspective on the analysis and design of M-CNNs, paving the way for advanced applications in edge computing and specialized hardware.

Keywords Memristor Cellular Nonlinear Networks · Vector Field · Valence Change Mechanism Memristors

1 Introduction

In the realm of computing, we find ourselves at the precipice of a significant paradigm shift. Traditional general-purpose computing systems are giving way to a new breed of specialized hardware, designed with utmost efficiency to tackle specific tasks. The driving force behind this transformative trend can be attributed to the heightened need for intelligent autonomous systems, specifically edge devices, which are capable of conducting sensing and processing tasks remotely. Consequently, these devices are constrained by a restricted power allocation and limited physical space.

The Cellular Nonlinear Network (CNN) is a widely recognized computer architecture that exhibits high levels of parallelism and possesses universal processing capabilities [1]. Standard CNN implementations are frequently employed for high-speed image processing tasks, which can be efficiently integrated into arrays of photo-sensors [2, 3]. In recent times, there has been a surge in interest surrounding memristors, which are novel electrical devices at the nanoscale level. These devices have garnered attention due to their exceptional characteristics, such as non-volatility, adaptability, low-power operation, and the ability to achieve high levels of integration [4–6]. The integration of memristor devices within CNN cells facilitated the storage of localized information within individual cells, thereby enhancing their dynamic characteristics [7–10].

Aiming to harness the unlimited processing capabilities of CNNs, Chua developed the Dynamic Route Map (DRM) representation as a theoretical tool to analyze 1st-order dynamical circuit behavior [11]. By utilizing this tool, individuals can effectively design and analyze the functioning of a CNN cell as a 1st-order dynamical system, thereby enabling the development of distinct processing operations. Moreover, a comprehensive analysis of a class of Memristor CNNs (M-CNN) has been presented in [7]. M-CNNs are obtained through the modification of conventional CNNs by incorporating a singular non-volatile memristor in parallel to the resistor-capacitor pair within each CNN cell. Considering the fact that the state evolution of the memristor contributes to the enhancement of cell's functionality, and taking into account the limitation of DRM-based analysis to 1st-order dynamical systems [12], it becomes apparent that examining the functionalities of 2nd-order processing elements within the aforementioned class with the DRM is no longer effective. Hence, the scope of the DRM graphical tool has been expanded to encompass nonlinear dynamical systems that possess two degrees of freedom [7]. This extension, referred to as 2nd-order DRM (DRM2) [7], draws inspiration from the Phase Portrait concept within the realm of nonlinear dynamics theory and illustrates the different regions within cell's phase plane on the basis of the sign of each cell state derivative. Nevertheless, the aforementioned tools do not incorporate the visualization of crucial information, such as the magnitude of each derivative that governs the local behavior of the cell.

In this present study, we aim to leverage the existing knowledge of the DRM and DRM2 analyses and tackle their limitations in order to achieve a more comprehensive expansion of these invaluable tools. In specific, we propose the integration of M-CNN cell's vector field within the graphical representation of the cell's Phase Portraits, thereby enhancing the efficacy of the design tool for the intricately dynamic M-CNN cells. Furthermore, we employ an accurate physics-based memristor model in order to face challenges associated with designing realistic M-CNN cells. These challenges include the logarithmic scale of memristor's state variable and significant magnitude scaling issues, which pose considerable difficulties in visualizing the vector field. The graphical analysis tool proposed here allows for a direct understanding of M-CNN cell's behavior and facilitates its efficient design.

2 M-CNN Cell Dynamics

Chua and Yang introduced the CNN architecture in their influential publication [13]. This framework involves a grid of interconnected cells that possess the capability to carry out computational tasks with high efficiency. Each CNN

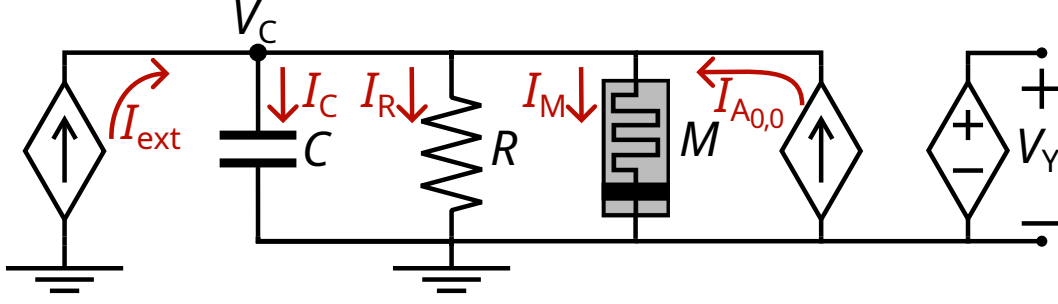


Figure 1: (a) M-CNN Cell's equivalent circuit.

cell $C_{i,j}$ consists of several components, including a resistor R , a capacitor C , and a self-feedback-dependent current source $I_{A_{0,0}}$, all connected in parallel, and an output voltage source V_Y (Fig. 1). The $R-C$ component is employed to form the state variable of each cell by charging and discharging the capacitor voltage V_C , while the source V_Y serves as the output signal of each cell, typically representing a nonlinear mapping of the state variable to a bounded output signal. Moreover, the self-feedback $I_{A_{0,0}}$ plays an important role on the computational operations of the CNN cell by regulating the stability of the cell.

The CNN cell functionality is completed by the extracell contributions, which consist of the weighted signals from the neighboring cells' inputs $V_{U|i,j}(t)$ and outputs $V_{Y|i,j}(t)$ and a fixed bias $I_{z|i,j}$, which are calculated as

$$I_{ext|i,j}(t) = \sum_{\substack{k=i-1, l=j-1 \\ (k,l) \neq (i,j)}}^{i+1, j+1} A_{k-i, l-j} V_{Y|k,l}(t) + \sum_{k=i-1, l=j-1}^{i+1, j+1} B_{k-i, l-j} V_{U|k,l}(t) + I_z.$$

The coefficients $B_{k-i, l-j}$ and $A_{k-i, l-j}$ are the coupling weights of $C_{i,j}$ with the input and output of $C_{k,l}$, respectively, where $k \in \{i-1, i, i+1\}$ and $l \in \{j-1, j, j+1\}$ for the standard CNN structure. Moreover, a factor z defines the independent current bias, such as $I_z = z$. For a space-invariant CNN, the complete set of weights $A_{k,l}$, $B_{k,l}$, and z for $k, l \in \{-1, 0, 1\}$ defines the CNN template, and its proper selection leads to different computational tasks.

An enhancement of conventional CNNs capabilities is achieved by integrating a distinct non-volatile memristor M in parallel to the $R-C$ pair within each CNN cell, forming the M-CNN architecture. Considering a realistic memristive device, like the Valence Change Mechanism (VCM) devices modeled by the Juelich-Aachen Resistive Switching Tool (JART) [14], the voltage- and state-dependent resistance of the cell's memristor R_M should be incorporated into cell's dynamics, constituting the following 2nd-order dynamical system

$$\dot{V}_C = \frac{dV_C}{dt} = \frac{I_{ext|i,j}(t) + I_{A_{0,0}}}{C} - \frac{V_C}{RC} - \frac{V_C}{R_M(V_C, N_d)C} \quad (1)$$

$$\dot{N}_d = \frac{dN_d}{dt} = -\frac{I_{ion}(V_C, N_d)}{z_{V_O} e A l_d} \quad (2)$$

where N_d is the state variable of the JART VCM memristor model, representing the concentration of oxygen vacancies in the vicinity of the interface between the switching layer and the active electrode of the device, named as the *disc region*. Moreover, l_d denotes the length of the disc region, z_{V_O} stands for the oxygen vacancy charge number, e represents the elementary charge and $A = \pi r_d^2$ defines the area of the switching filament. The ionic current I_{ion} represents the current of the moving oxygen vacancies during memristor's switching and it depends on N_d and the applied voltage, as elaborated in [15]. For the calculation of R_M , the explicit memristor current equation from the simplified JART VCM model [16] is used since it offers faster and more stable memristor current calculation.

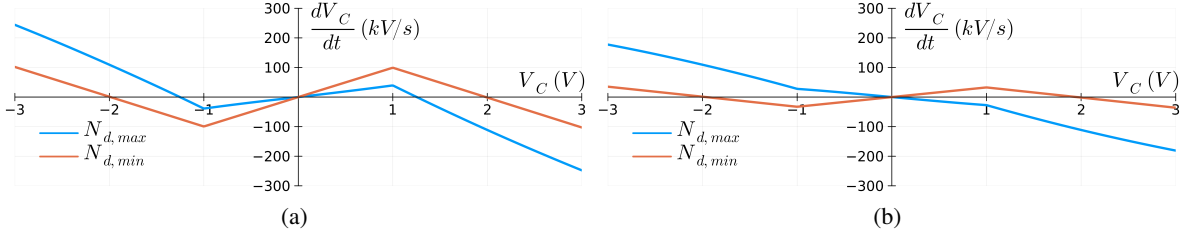


Figure 2: Illustration of M-CNN Cell's SDRs for $N_d = N_{d,min}$ and $N_d = N_{d,max}$ with R selected as (a) $R = 1 \text{ k}\Omega < R_{M,min} < R_{M,max}$ and, (b) $R_{M,min} < R = 3 \text{ k}\Omega < R_{M,max}$.

3 M-CNN Cell Dynamics Analysis

Aiming to delve deeper into the cell dynamics, enriched by the incorporation of a memristor device, the context of this work is focused on the isolated M-CNN cell, where $I_{ext|i,j}(t) = 0$, so all the template weights are zero, apart from the cell's self-feedback weight $A_{0,0}$.

Let us consider a typical M-CNN cell configuration, where $I_{A_{0,0}} = A_{0,0}V_Y/R$ with $A_{0,0} = 2$ and

$$V_Y = F_Y(V_C) = \frac{1}{2} (|V_C + 1| - |V_C - 1|). \quad (3)$$

If R is properly selected such as $R < R_{M,min} < R_{M,max}$ ², the M-CNN cell exhibits bistable behavior regardless memristor's state. In that case, both the State Dynamic Route (SDR) for the lowest and the highest N_d values, shown in Fig. 2(a), consist of a three-piece piecewise linear function with the middle piece having positive slope. Employing, first, conventional CNN analysis techniques, we investigate cell's equilibria, where $\dot{V}_C = 0V/s$, for theoretical non-dynamical memristors, i.e. $\dot{N}_d = 0$ always. So, each of those SDRs shows one unstable equilibrium at $V_C = 0V$ and two stable equilibria, one at negative and one at positive V_C values.

On the other hand, if R is selected such as $R_{M,min} < R < R_{M,max}$, the SDR for $N_d = N_{d,max}$ changes shape such that the middle piece admits negative slope, as shown in Fig. 2(b). As a result, the M-CNN cell for $N_d = N_{d,max}$ has only one equilibrium point at $V_C = 0V$ and it is a stable one.

Memristors are dynamical elements and the above analysis method is limited to the cases that memristor's dynamics are much faster than capacitor's ones, such that memristor is abruptly switching between $N_{d,min}$ and $N_{d,max}$. In that case, the whole M-CNN cell's behavior can be illustrated by the transition from one SDR to the other, when memristor switches. For M-CNN cells with fast capacitors or/and memristor devices with gradual switching properties, an analysis technique that incorporates the whole range $N_{d,min} \leq N_d \leq N_{d,max}$ should be employed.

In that case, where M-CNN cell cannot be simplified to a 1st-order system, the 2nd-order system (1)-(2) should be visualized in its complete phase plane, where $N_d \in [N_{d,min}, N_{d,max}]$ and $V_C \in [V_{C,min}, V_{C,max}]$. Since there is no strict limitation on V_C value, we select here $V_C \in [-3V, 3V]$. Fig. 3 illustrates separately the capacitor dynamics (Fig. 3(a)-(b)) and the memristor dynamics (Fig. 3(c)) in the 2d phase plane. The dynamics of cell's capacitor and memristor are interdependent, so, their separate illustration does not allow for the analysis of M-CNN cell's behavior.

For that reason, the DRM2 tool [7] combines them into a single illustration by using the sign of each derivative, leading to four regions with all the combinations of positive and negative capacitor's voltage derivative and memristor's state derivative. Unfortunately, by only using the sign, the information on the magnitude of each derivative is missing and, as a result, the DRM2 tool does not facilitate the direct visualization of M-CNN cell's dynamical behavior, requiring for the addition of trajectory lines on the same plot, which are generated by simulating the cell for various initial conditions.

In this paper, we extend this graphical analysis tool by incorporating the illustration of cell's vector field into its phase plane. The vector field of a 2nd-order system refers to the mapping that describes how the derivatives of the state variables depend on the current state of the system. This current state refers to each $\{V_C, N_d\}$ pair in the phase plane, while the local derivative values define the magnitude and the angle of an arrow (vector) that shows the direction along which the cell state will evolve.

²When N_d is at its lowest (highest) value $N_{d,min}$ ($N_{d,max}$) we observe $R_{M,max}$ ($R_{M,min}$).

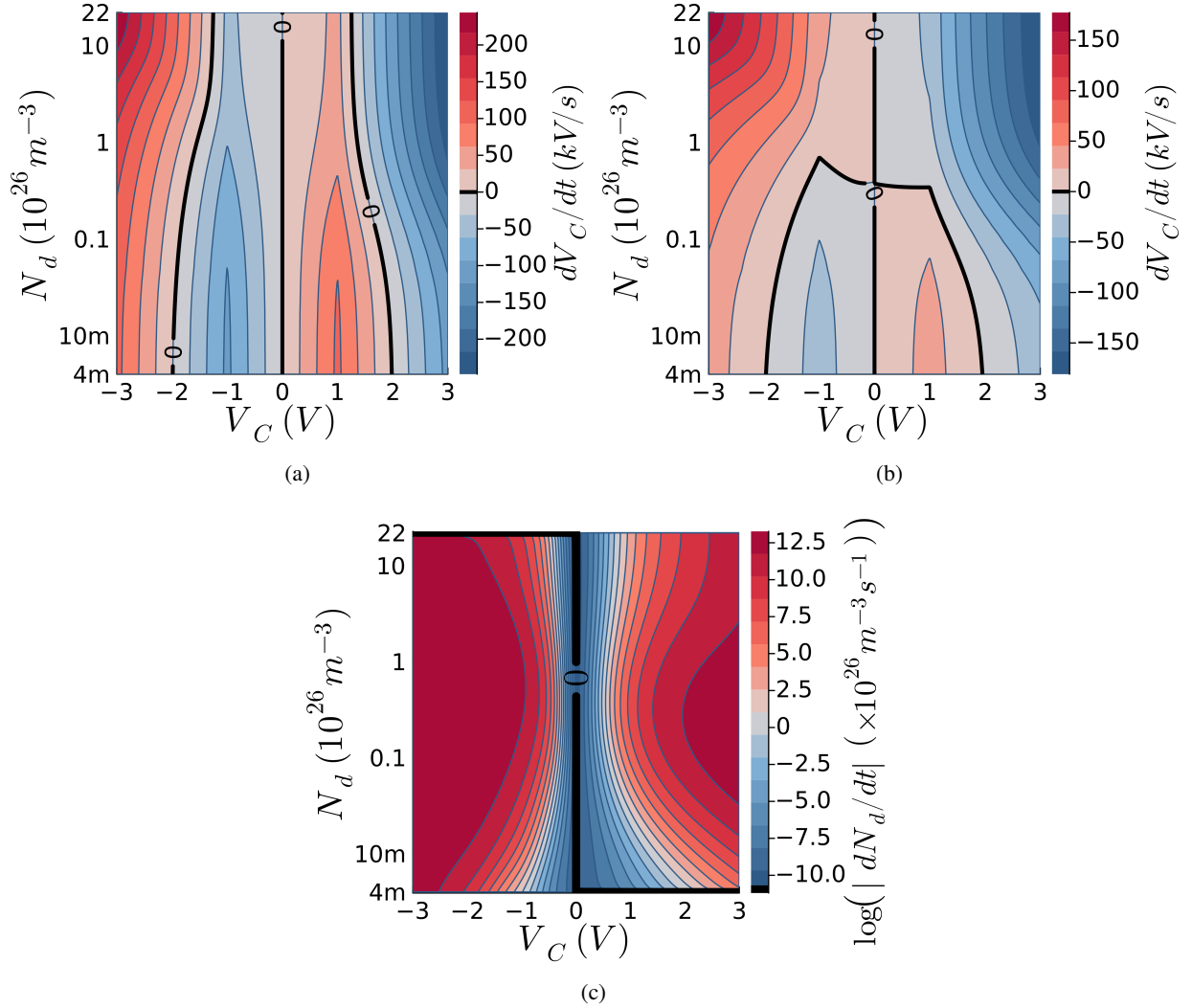


Figure 3: Capacitor voltage derivative for (a) $R = 1 \text{ k}\Omega < R_{M,\min} < R_{M,\max}$, and (b) $R_{M,\min} < R = 3 \text{ k}\Omega < R_{M,\max}$, and (c) memristor state derivative within M-CNN cell's phase plane.

Deriving the vector field for the M-CNN cell dynamics constitutes a tricky task since the two state equations exhibit big scaling differences, as well as memristor dynamics individually shows differences of many orders of magnitude for different V_C values. Based on that, we propose the normalization of arrow's magnitude, since information cannot be efficiently coded on its exact value. In our approach, all the vectors' lengths are the same, lying always on an ellipse with fixed vertical and horizontal radii, while the arrow's angle is calculated via the two state derivatives, such that

$$\theta(V_C, N_d) = \tan^{-1} \left(\frac{\dot{N}_d(V_C, N_d)}{\dot{V}_C(V_C, N_d)} \right) \quad (4)$$

Moreover, in order to incorporate the missing information of vector's magnitude into the arrow, we encode it to the coloring of the arrow. Such that, the arrow color is selected based on the 2-norm, also known as Euclidean norm, of the vector at each phase plane point.

In addition, moving from the 1st-order DRM where the zero crossings constitute equilibrium points, the proposed 2nd-order illustration shows also the corresponding points, known as nullclines, for V_C by dashed black line and N_d by dotted gray line. The equilibria for the 2nd-order cell appear at the crossings of the V_C and N_d nullclines. The points along the locus $dV_C/dt = 0$, which correspond to stable equilibria for the CNN cell (as well as for the M-CNN

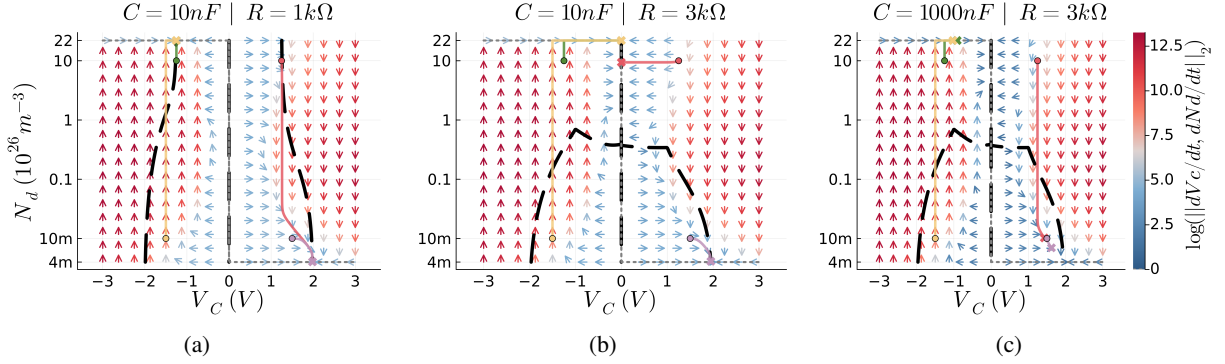


Figure 4: Enhanced graphical illustration of M-CNN cell's dynamics including the cell's vector field. (a) Fully bistable M-CNN cell design. (b)-(c) Hybrid mono- and bistable M-CNN cell design for different C values. In all plots, the V_C and N_d nullclines are illustrated in blue dashed and gray dotted lines, respectively, while the solid lines are cell trajectories starting from the circle marker at $\{V_{C,0}, N_{d,0}\}$ and end at the cross marker at $\{V_{C,t}, N_{d,t}\}$ after a simulation with duration $t = 1$ ms.

cell, in those scenarios where its memristor operates as an adynamic resistive element [7]), attract locally phase-plane solution trajectories for the n^{d} -order M-CNN cell. The plots in Fig. 4 illustrate the application of the proposed dynamical analysis graphical tool for the investigation of M-CNN cell's behavior. The colored solid lines are the trajectories of the cell starting from a selected initial $\{V_{C,0}, N_{d,0}\}$ point and simulated for certain time ($t = 1$ ms).

Fig. 4(a) illustrates the proposed graphical analysis tool for a M-CNN cell with $R < R_{M,min} < R_{M,max}$, where the cell's dynamics exhibit always bistable behavior, which is evident from the shape of the nullclines. On the other hand, Fig. 4(b) demonstrates the case where $R_{M,min} < R < R_{M,max}$, and mono- and bistability coexist. In that case, the arrows directly illustrate the direction that cell states will follow, making evident the transition path from bistability to monostability of capacitor voltage's dynamics. One more example is shown in Fig. 4(c), where the cell's design is the same, apart from the capacitance value of cell's capacitor. That change affects the relationship between capacitor's and memristor's switching speed, leading to a direct change to some arrows' angle. As it is evident when comparing Fig. 4(b) with Fig. 4(c), the trajectories of some initial conditions exhibit different behaviors, e.g. the red lines ($\{V_{C,0} = 1.25\text{V}, N_{d,0} = 10 \times 10^{26}\text{m}^{-3}\}$). Those different behaviors are directly illustrated by our proposed method, however, they could not be shown in a DRM, but also the DRM2 tool is not able to naturally illustrate them, since it is limited to the sign of the derivatives only.

4 Conclusions

In the present manuscript, we propose a novel graphical representation for the purpose of analyzing the 2^{nd} -order M-CNN cell. Drawing inspiration from the widely recognized DRM and DRM2 graphical illustration tools, a novel and sophisticated tool is postulated, wherein the system's vector field are seamlessly integrated into the complete phase plane. With the utmost intention of accentuating the merits inherent in the proposed methodology, we hereby present a comprehensive exposition of the isolated M-CNN cell's dynamics across a multitude of scenarios, wherein the advantages of the vector field representation are unequivocally discernible.

5 Acknowledgments

This work was supported in part by the Deutsche Forschungsgemeinschaft within the project SPP2622 Mem2CNN, in part by the Federal Ministry of Education and Research (BMBF, Germany) in the project NEUROTEC II (project numbers 16ME0398K and 16ME0399), and in part by NeuroSys A with the Ref.No: 03ZU1106AA.

References

- [1] L. O. Chua, *CNN: A paradigm for complexity*. World Scientific, 1998, vol. 31.
- [2] L. O. Chua and T. Roska, *Cellular neural networks and visual computing: foundations and applications*. Cambridge university press, 2002.

- [3] A. Rodriguez-Vazquez, J. Fernandez-Berni, J. A. Lenero-Bardallo, I. Vornicu, and R. Carmona-Galan, "CMOS vision sensors: Embedding computer vision at imaging front-ends," *IEEE Circuits and Systems Magazine*, vol. 18, no. 2, pp. 90–107, 2018.
- [4] R. Tetzlaff, *Memristors and memristive systems*. Springer, 2013.
- [5] A. Siemon, T. Breuer, N. Aslam, S. Ferch, W. Kim, J. Van Den Hurk, V. Rana, S. Hoffmann-Eifert, R. Waser, S. Menzel *et al.*, "Realization of boolean logic functionality using redox-based memristive devices," *Advanced functional materials*, vol. 25, no. 40, pp. 6414–6423, 2015.
- [6] A. Ascoli, S. Menzel, V. Rana, T. Kempen, I. Messaris, A. S. Demirkol, M. Schulten, A. Siemon, and R. Tetzlaff, "A deep study of resistance switching phenomena in TaOx ReRAM cells: System-theoretic dynamic route map analysis and experimental verification," *Advanced Electronic Materials*, vol. 8, no. 8, p. 2200182, 2022.
- [7] R. Tetzlaff, A. Ascoli, I. Messaris, and L. O. Chua, "Theoretical foundations of memristor cellular nonlinear networks: Memcomputing with bistable-like memristors," *IEEE Transactions on Circuits and Systems I: Regular Papers*, vol. 67, no. 2, pp. 502–515, 2019.
- [8] A. Ascoli, I. Messaris, R. Tetzlaff, and L. O. Chua, "Theoretical foundations of memristor cellular nonlinear networks: Stability analysis with dynamic memristors," *IEEE Transactions on Circuits and Systems I: Regular Papers*, vol. 67, no. 4, pp. 1389–1401, 2019.
- [9] I. Messaris, A. Ascoli, A. S. Demirkol, R. Tetzlaff, and L. Chua, "Multi-tasking and memcomputing with memristor cellular nonlinear networks," in *2020 27th IEEE International Conference on Electronics, Circuits and Systems (ICECS)*. IEEE, 2020, pp. 1–4.
- [10] A. Ascoli, R. Tetzlaff, S.-M. Kang, and L. O. Chua, "Theoretical foundations of memristor cellular nonlinear networks: A DRM2-based method to design memcomputers with dynamic memristors," *IEEE Transactions on Circuits and Systems I: Regular Papers*, vol. 67, no. 8, pp. 2753–2766, 2020.
- [11] L. Chua, "Five non-volatile memristor enigmas solved," *Applied Physics A*, vol. 124, pp. 1–43, 2018.
- [12] V. Ntinis, Y. Wang, A. S. Demirkol, I. Messaris, V. Rana, S. Menzel, A. Ascoli, and R. Tetzlaff, "Design and analysis of isolated voltage-mode memristor cellular nonlinear network cells," in *2023 IEEE International Symposium on Circuits and Systems (ISCAS)*. IEEE, 2023, pp. 1–5.
- [13] L. Chua and L. Yang, "Cellular neural networks: theory," *IEEE Transactions on Circuits and Systems*, vol. 35, no. 10, pp. 1257–1272, Oct. 1988. [Online]. Available: <https://ieeexplore.ieee.org/document/7600/>
- [14] C. Bengel, A. Siemon, F. Cüppers, S. Hoffmann-Eifert, A. Hardtdegen, M. von Witzleben, L. Hellmich, R. Waser, and S. Menzel, "Variability-aware modeling of filamentary oxide-based bipolar resistive switching cells using SPICE level compact models," *IEEE Transactions on Circuits and Systems I: Regular Papers*, vol. 67, no. 12, pp. 4618–4630, 2020.
- [15] V. Ntinis, A. Ascoli, I. Messaris, Y. Wang, V. Rana, S. Menzel, and R. Tetzlaff, "Toward simplified physics-based memristor modeling of valence change mechanism devices," *IEEE Transactions on Circuits and Systems II: Express Briefs*, vol. 69, no. 5, pp. 2473–2477, 2022.
- [16] V. Ntinis, D. Patel, Y. Wang, I. Messaris, V. Rana, S. Menzel, A. Ascoli, and R. Tetzlaff, "A simplified variability-aware vcm memristor model for efficient circuit simulation," in *2023 19th International Conference on Synthesis, Modeling, Analysis and Simulation Methods and Applications to Circuit Design (SMACD)*. IEEE, 2023, pp. 1–4.